DOI: 10.61782/fa.2025.0271

FORUM ACUSTICUM EURONOISE 2025

DESIGN AND EXPERIMENTAL CHARACTERIZATION OF MULTI-MODAL METAMATERIAL PANELS ACHIEVING BROADBAND SOUND TRANSMISSION AND RADIATION REDUCTION

Daniele Giannini[1]* **Lucas Van Belle**[2,3] **Elke Deckers**[3,4]
Edwin P.B. Reynders[1]
[1] Department of Civil Engineering, KU Leuven, Belgium
[2] Department of Mechanical Engineering, KU Leuven, Belgium
[3] Flanders Make@KU Leuven, Belgium
[4] Department of Mechanical Engineering, Campus Diepenbeek, KU Leuven, Belgium

ABSTRACT

Resonant metamaterials are a promising approach to achieve vibroacoustic attenuation in partition panels. By adding subwavelength resonators to a host plate, free-travelling elastic waves in specific frequency bands, called bandgaps, are prohibited. While conventional resonant metamaterials typically exploit single-mode translational resonators resulting in narrowband attenuation, recent advancements have theoretically indicated that broader attenuation bands can be achieved by resonators with multiple translational and rotational modes. However, the effectiveness of this concept has not yet been experimentally demonstrated. In this study, we address this gap by designing, manufacturing and experimentally validating a multi-modal metamaterial panel aimed at mitigating broadband coincidence effects in orthotropic host plates. The proposed metamaterial panel integrates medium-density fiberboard resonators attached to an orthotropic cross-laminated timber plate. The resonator geometry is optimized to maximize the effect of two distinct directional bandgaps induced by two rotational resonator modes. Extensive vibroacoustic testing is performed to characterize the metamaterial performance. Laser vibrometry measurements under shaker-based excitation confirm the presence of these two resonance-based bandgaps. Sound transmission and radiation tests demonstrate significant attenuation within the bandgaps (by around 8-10 dB) compared to the host plate, as well as the suppression of the broad sound transmission loss dip due to coincidence effects.

Keywords: *locally resonant metamaterial panels, multi-modal resonators, sound transmission loss, sound radiation, experimental characterization*

1. INTRODUCTION

In the search for compact and lightweight solutions for vibroacoustic attenuation, locally resonant metamaterials have been introduced to achieve exceptional properties beyond those of conventional materials [1]. These metamaterials achieve enhanced wave control by small, local resonators added to a host structure on a subwavelength scale. As a result, an effective mass that varies with frequency is achieved, which shows a peak around the local resonance [2]. Around this frequency, the effective mass of the metamaterial structure surpasses its static mass, significantly improving sound insulation [3, 4]. Additionally, in the frequency range immediately above the peak, the effective mass becomes negative and a wave propagation bandgap emerges, which inhibits free-traveling mechanical waves [5].

Metamaterials have been successfully employed to enhance vibration attenuation and sound insulation in partition panels [6]. Conventional designs only utilize a single mode of the local resonators, typically associ-

*__Corresponding author__: daniele.giannini@kuleuven.be.

ated with a transversal vibration to the host plate, therefore limiting the attenuation bandwidth. To achieve attenuation in a broader band, multiple mechanical resonators can be attached in series [7, 8] or in parallel [9, 10] to the host plate. More recently, theoretical studies have indicated that multi-modal metamaterial panels—featuring multiple local resonances within each resonating unit, and including both transversal and rotational modes—can generate a sequence of adjacent attenuation bands, which collectively span a broader frequency range [11, 12]. However, despite their potential, the experimental validation of metamaterial panels incorporating multi-modal and particularly rotational resonators remains an open challenge.

This study addresses this gap by designing, manufacturing and experimentally validating a metamaterial panel with multi-modal rotational resonators. The proposed metamaterial panel is specifically tailored to mitigate broadband coincidence effects in orthotropic host plates. It consists of a host orthotropic plate made of cross-laminated timber (CLT) to which local resonators made of medium-density fiberboard (MDF) are attached. The resonator geometry is optimized to suppress the broad sound transmission loss (STL) dip due to coincidence effects in the host panel, by leveraging two distinct directional bandgaps induced by two rotational resonator modes. Extensive vibroacoustic testing is conducted to assess the performance of the metamaterial panel, in terms of sound transmission loss, structural wave propagation, and sound radiation.

The paper is structured as follows. Section 2 describes the design of the proposed multi-modal metamaterial CLT panel. The experimental validation is presented in the following Sections, in terms of sound transmission loss (Section 3), flexural wave propagation (Section 4), and sound radiation (Section 5). Finally, Section 6 concludes the paper.

2. DESIGN OF THE MULTI-MODAL METAMATERIAL CLT PANEL

The proposed metamaterial panel, shown in Fig. 1, consists of an orthotropic CLT host plate with periodically attached multi-modal rotational resonators made of MDF. The orthotropic host CLT panel is composed of 3 spruce wood layers, crosswise glued together with alternating fiber directions [13], following a 0°/90°/0° stacking sequence relative to the global x-axis. The host CLT panel has an overall thickness of $t_{\mathrm{CLT}} = 0.027$ m

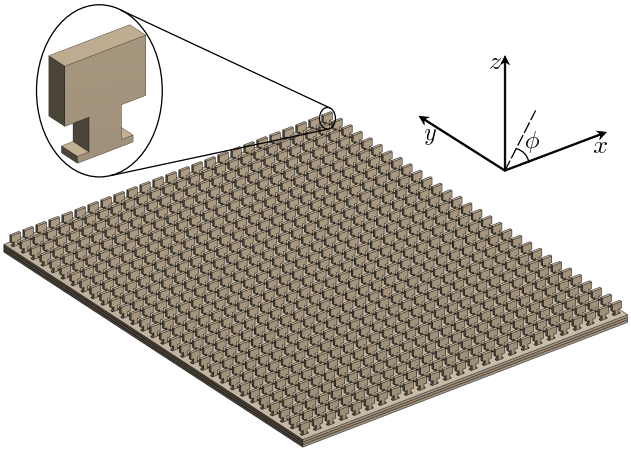

Figure 1: Designed metamaterial CLT panel with MDF multi-modal rotational resonators.

(each layer being 0.009 m thick), and has in-plane dimensions 1.235×1.485 m^2.

Due to its high degree of orthotropy, the host CLT panel exhibits broadband coincidence effects, leading to a broad dip in its diffuse STL curve. In orthotropic panels, the critical frequency f_{cr}, at which the flexural wave speed matches the speed of sound waves in the surrounding fluid, varies with the in-plane propagation direction defined by the azimuthal angle ϕ (see Fig. 1). Under diffuse sound incidence, this results in a broad coincidence STL dip spanning the range $\left[\min\left(f_{\mathrm{cr}}(\phi)\right), \max\left(f_{\mathrm{cr}}(\phi)\right)\right]$. To mitigate broadband coincidence effects, the metamaterial panel integrates multi-modal local resonators made of MDF. The resonators are laser-cut and periodically attached to the host panel using adhesive, with subwavelength unit cell dimensions 0.05×0.05 m^2. Each resonator includes a vertical cantilever beam, a mass at the top of the beam, and a broadened base for attachment to the host panel.

The material properties of the CLT layers and the MDF resonators are experimentally identified through dynamic testing [14] and summarized in Tab. 1. Both materials are modelled as orthotropic and characterized by the Young's moduli E_{x}, E_{y}, E_{z}, the shear moduli G_{xy}, G_{yz}, G_{xz}, the Poisson's ratios ν_{yx}, ν_{zy}, ν_{zx}, the mass density ρ, and the damping loss factor η.

The multi-modal local resonators are designed to suppress the broad STL dip of the host structure. This is performed by leveraging the first two bending modes of the vertical cantilever beam-mass structure (Fig. 2),

Table 1: Estimated material properties for CLT layers and MDF. CLT properties refer to the local reference system, with x-axis along the wood fibers, oriented at 0°/90°/0° to the global x-axis. MDF properties refer to the global reference system.

	CLT layers	MDF
$E_x = E_z$ [N/m^2]	$6.8 \cdot 10^8$	$3.67 \cdot 10^9$
E_y [N/m^2]	$1.202 \cdot 10^{10}$	$2.65 \cdot 10^8$
$G_{xy} = G_{yz}$ [N/m^2]	$8.3 \cdot 10^8$	$1.55 \cdot 10^8$
G_{xz} [N/m^2]	$7.12 \cdot 10^7$	$1.31 \cdot 10^9$
$\nu_{yx} = \nu_{zy}$ [-]	0.0189	0.0672
ν_{zx} [-]	0.03	0.25
ρ [kg/m^3]	468	616
η [-]	0.07	0.025

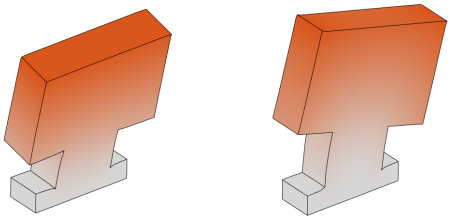

Figure 2: Eigenmodes of the local resonator at 1085 Hz and 1640 Hz.

in which the end mass rotates around the x and the y axis respectively. These rotational modes generate two directional bandgaps that inhibit flexural wave propagation in the directions perpendicular to the rotation axes, and are exploited to suppress coincidence effects along the two principal axes of the orthotropic host plate.

The resonator layout is numerically optimized by using the dimensions of its geometrical features as design variables. A genetic algorithm is employed to maximize the broadband diffuse STL in the frequency range 100-3150 Hz, while ensuring that the resonator mass does not exceed 20% of the host panel's mass [11]. The final optimized configuration exhibits local resonance frequencies at 1085 Hz and 1640 Hz (Fig. 2), strategically positioned to suppress the broad STL dip, and maximized participating mass in the modes of interest.

Figure 3: Fabricated multi-modal metamaterial panel, mounted in the transmission opening of the Laboratory of Acoustics of KU Leuven.

3. EXPERIMENTAL EVALUATION OF THE SOUND TRANSMISSION LOSS

The STL of both the bare CLT host panel and the metamaterial panel is experimentally measured in the transmission suite of the Laboratory of Acoustics of KU Leuven. The facility consists of two reverberation chambers, each with a volume of 87 m^3, and a transmission opening with dimensions 1.25 × 1.5 m^2, inside which the tested panel is installed (Fig. 3). The sound transmission loss R is measured according to the ISO 10140-2 standard [15].

The STL curves of the bare CLT panel (without resonators) and the metamaterial CLT panel are displayed in 1/48-octave bands in Fig. 4, along with numerical predictions obtained through an infinitely periodic finite element model [16, 17]. In this model, one single unit cell is discretized by solid finite elements, including a segment of the laminated CLT panel and one attached resonator. The STL is computed by analyzing the interaction between the panel and the surrounding diffuse acoustic fields, under appropriate periodicity boundary conditions. The numerical predictions are reported for the bare panel, for a bare panel with an equivalent

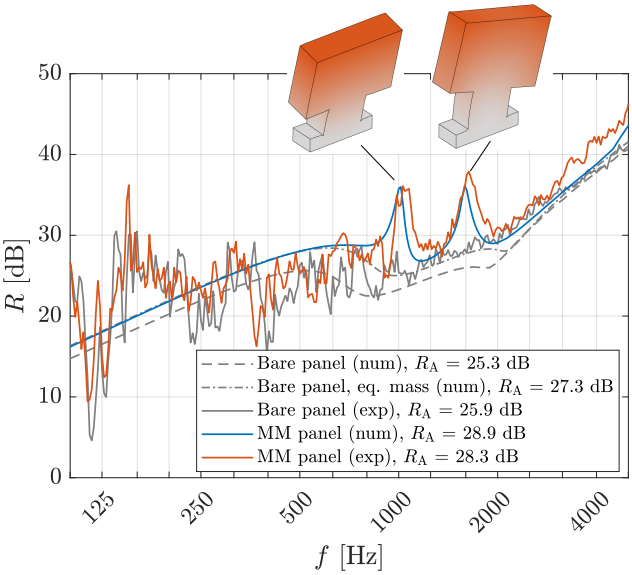

Figure 4: Comparison between the experimentally measured and numerically predicted diffuse STL of the bare and the metamaterial panel.

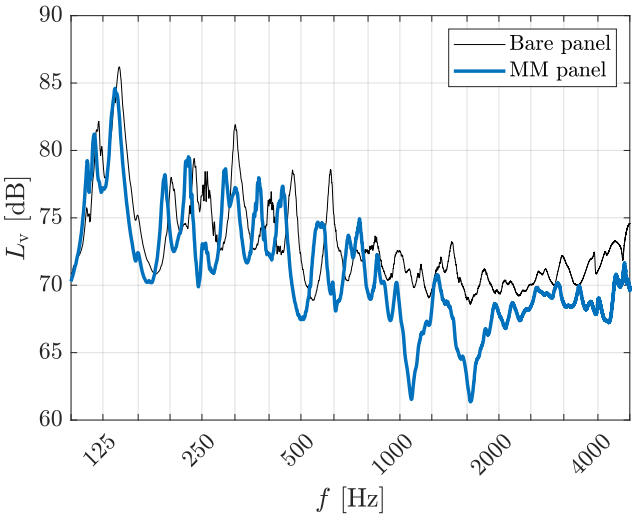

Figure 5: Comparison between the experimentally measured surface-averaged vibration velocity levels of the bare and the metamaterial panel under shaker-based excitation.

mass to the metamaterial panel, and for the metamaterial panel.

At low frequencies, the 20% added mass of the resonators shifts the numerical STL curve upwards by around 1.6 dB. In this range, besides mass effects, the measured STL is mainly dominated by the global modal behaviour of the panel, which is particularly prominent given its relatively compact dimensions. Since the periodic finite element model does not account for boundary effects and global panel resonances, some deviations between numerical and experimental results are observed.

Above 250 Hz, the influence of the individual panel modes becomes less significant, progressively leading to a good alignment between numerical predictions and experimental results. Within the broad coincidence range (760-1950 Hz), the STL dip observed in the bare panel is effectively suppressed by two distinct STL peaks, achieving STL improvements of about 8-10 dB around the local resonance frequencies. Interestingly, no STL dip is observed in the frequency ranges immediately above the resonance peaks, which constrasts with the usual behaviour seen when the local resonances are tuned below coincidence. By tuning the local resonances within the coincidence range, here no additional range of increased radiation efficiency is introduced, and the overall zone of efficient acoustic radiation is reduced [18].

To provide a standardized evaluation of the sound insulation performance, the single number rating R_A from ISO 717 [19] is also computed. This metric represents the A-weighted broadband diffuse sound insulation for pink noise excitation over the frequency range 100-3150 Hz, and is found as $R_A = R_w + C$, where R_w and C are defined by the ISO standard. Both numerical predictions and experimental results indicate that the metamaterial panel achieves an increase of R_A by around 3 dB compared to the bare CLT panel, while the R_A improvement with respect to the bare panel with equivalent mass is 1.6 dB. This confirms the effectiveness of the proposed multi-modal rotational resonator design in enhancing broadband sound insulation.

4. EXPERIMENTAL EVALUATION OF FLEXURAL WAVE PROPAGATION

To evaluate the impact of the metamaterial design on flexural wave dispersion, the vibration fields in both the bare CLT panel and the metamaterial panel are measured under shaker excitation. The shaker is attached to the panel (mounted in the transmission opening) via

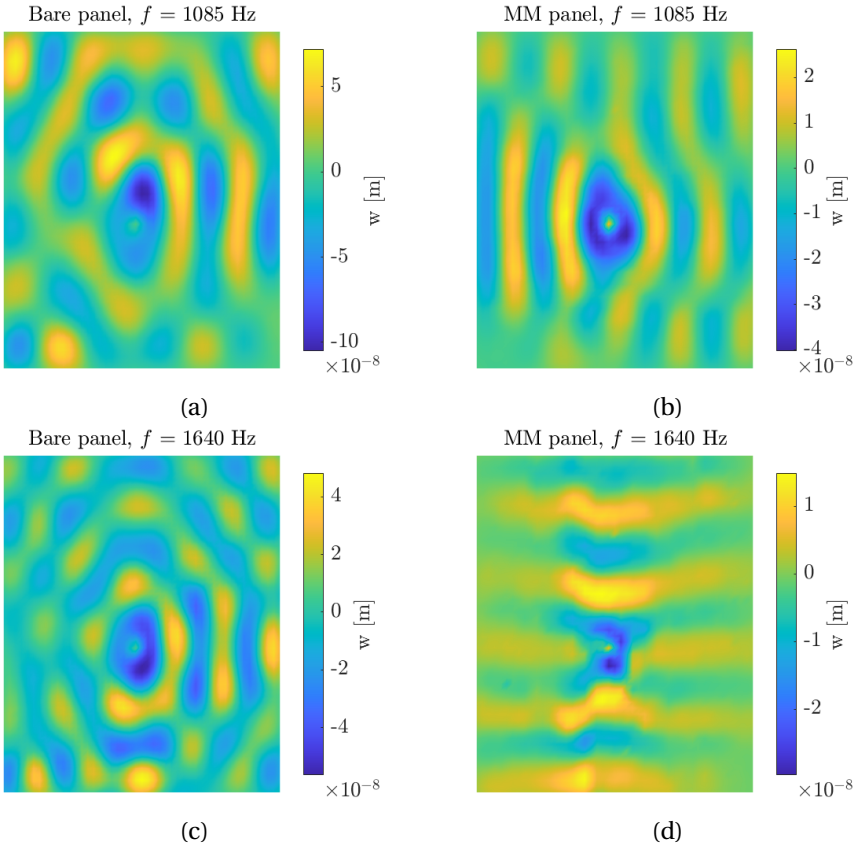

Figure 6: Measured vibration fields for (a, c) the bare and (b,d) the metamaterial panel at (a,b) 1085 Hz and (c,d) 1640 Hz, in terms of the out-of-plane displacement w.

an impedance head, which measures the input force. The shaker is positioned slightly off-centered with respect to the panel, and a white noise excitation signal is applied as input. The resulting out-of-plane vibration field is measured by a scanning laser Doppler vibrometer (SLDV), by evaluating the frequency response function (FRF) between the input force and the displacement responses. A Polytec PSV-Qtec Scanning Vibrometer is used to capture the vibration field at 2769 points on a rectangular grid, with a spatial resolution of 2.5 cm. Measurements are taken across the frequency range 0-6400 Hz with a frequency resolution of 0.5 Hz.

The measured vibration data are used to compute the surface-averaged velocity level L_v at each frequency, considering a reference velocity value of $5 \cdot 10^{-8}$ m/s. Fig. 5 compares the L_v curves for the bare panel and the metamaterial panel, in 1/48-octave bands. Across the entire frequency range, the added mass of the resonators causes a slight shift downwards in the L_v curve of the metamaterial panel compared to the bare CLT panel, along with a slight reduction of the resonance frequencies associated with the global panel modes. Most notably, two pronounced dips appear at 1085 Hz and 1640 Hz, corresponding to the directional bandgaps introduced by the local resonators. Around these frequencies, the vibration levels are effectively reduced by approximately 8 dB compared to the bare panel.

The impact of the directional bandgaps is further analyzed by comparing the measured vibration fields of the metamaterial panel against those of the bare panel. In the bare panel, flexural waves radiate uniformly in all directions from the excitation point (Figs. 6a and 6c). In the metamaterial panel, wave propagation is inhibited in specific directions due to the introduced directional

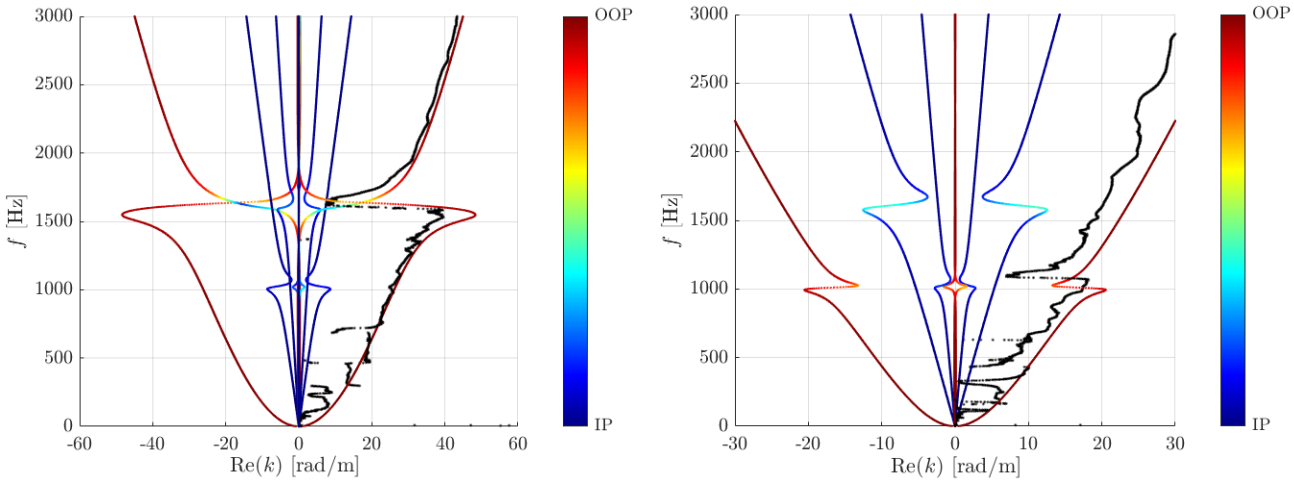

Figure 7: Experimental (black) and numerical (coloured) dispersion curves of the metamaterial panel for propagation along (a) the x axis and (b) the y axis. The numerical dispersion curves are coloured according to the out-of-plane (OOP) vs. in-plane (IP) nature of the wave modes.

bandgaps: at 1085 Hz, flexural wave propagation is suppressed along the vertical direction (Fig. 6b), while at 1640 Hz, flexural wave propagation is suppressed along the horizontal direction (Fig. 6d).

To further characterize the wave behaviour, the experimental dispersion curves are extracted using the Extended Inhomogeneous Wave Correlation approach [5], which correlates the measured vibration fields with analytical functions representing inhomogeneous plane waves. Fig. 7 presents the experimental dispersion curves (for real wavenumbers), along with numerical predictions through periodic finite element modelling. The numerical dispersion curves are coloured according to the out-of-plane nature of the wave modes, which is calculated using the ratio of surface-averaged out-of-plane to in-plane nodal displacements at the mid-plane of the plate: red indicates out-of-plane flexural waves and blue indicates in-plane waves. Both in-plane and out-of-plane (flexural) dispersion branches are numerically predicted, but since only out-of-plane displacement fields are measured, only the flexural wave dispersion is experimentally retrieved.

In the lower frequency range, the experimental estimation of the dispersion curves is strongly influenced by the global modal behaviour of the panel. Above 800 Hz, the modal behaviour of the panel becomes less pronounced, and a good agreement is observed between experimental and numerical results. A minor discrepancy is present in the slope of the dispersion curve for propagation along y, where the experimental panel appears slightly stiffer than predicted.

For both numerical and experimental results, two regions of significant flexural wave dispersion are identified: one around the first directional bandgap for propagation along y and another around the second directional bandgap for propagation along x. The observed bandgap behavior shows strong agreement between experimental measurements and numerical simulations.

Interestingly, the numerical model further predicts that the directional bandgaps also affect in-plane wave propagation, despite this effect not being captured by experiments. This highlights that the designed vertical cantilever beam-mass resonators transfer both bending moments and in-plane forces to the host structure, impacting both flexural and in-plane wave behavior.

5. EXPERIMENTAL ASSESSMENT OF SOUND RADIATION

To experimentally assess the reduction of acoustic radiation in the bandgap regions, the spatially averaged sound pressure in the receiver room of the transmission

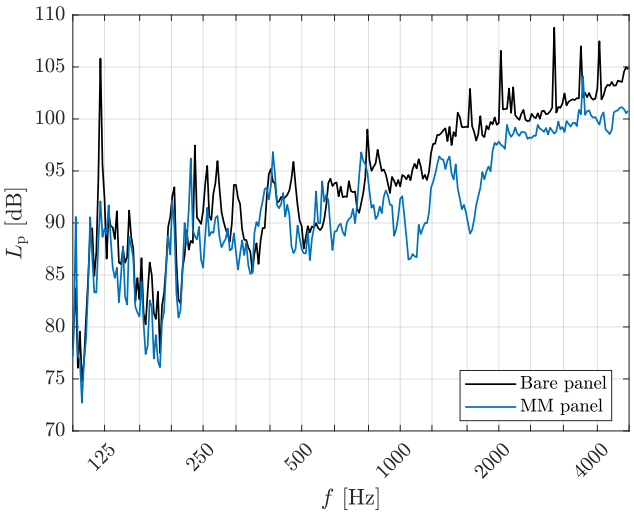

Figure 8: Comparison between the experimentally measured sound pressure levels in the receiver room when the bare and the metamaterial panel are subjected to structure-borne (point) excitation.

suite is measured, when the panel is mounted in the transmission opening and subjected to structure-borne (point) shaker excitation. The FRF between the input shaker force and the harmonic sound pressure in the receiver room is measured for 4 different excitation locations and 8 microphone locations. The sound pressure level L_p per unit of excitation force is then computed by energetically averaging the FRFs obtained for all excitation and measurement positions.

Fig. 8 compares the resulting sound pressure levels for the bare panel and the metamaterial panel, in 1/48-octave bands. In general, the metamaterial panel exhibits a slight reduction in overall sound radiation due to the additional mass of the resonators. More significantly, two distinct dips are observed around the local resonance frequencies (1085 Hz and 1640 Hz), where the metamaterial treatment achieves an 8–10 dB reduction in radiated sound pressure compared to the bare CLT panel.

6. CONCLUSIONS

In this work, we have experimentally demonstrated the effectiveness of multi-modal metamaterial panels in achieving broad attenuation bands. Specifically, a multi-modal metamaterial panel has been designed, manufactured and experimentally validated to mitigate broadband coincidence effects in orthotropic host plates. The proposed metamaterial panel integrates medium-density fiberboard resonators attached to an orthotropic cross-laminated timber plate. The resonators consist of a vertical cantilever beam-mass structure and their layout has been geometrically optimized to maximize the effect of two distinct directional bandgaps induced by two rotational modes.

The performance of the metamaterial panel has been characterized by extensive vibroacoustic testing. Laser vibrometry measurements under shaker-based excitation have confirmed the presence of two resonance-based bandgaps. Diffuse sound transmission and radiation tests have demonstrated significant attenuation within the bandgaps (by around 8-10 dB) compared to the host plate, as well as the suppression of the broad sound transmission loss dip caused by coincidence effects.

The results of the work represent a significant advancement towards lightweight insulating partitions with broadband enhanced vibroacoustic performance through metamaterials.

7. ACKNOWLEDGEMENTS

Daniele Giannini and Lucas Van belle gratefully acknowledge the financial support of Research Foundation - Flanders (FWO), respectively through the post-doctoral fellowships 12A3Q24N and 1254325N. Furthermore, this work was supported by KU Leuven internal funds under project C2E/24/031.

8. REFERENCES

[1] G. Ma and P. Sheng, "Acoustic metamaterials: From local resonances to broad horizons," *Science Advances*, vol. 2, no. 2, p. e1501595, 2016.

[2] P. Li, S. Yao, X. Zhou, G. Huang, and G. Hu, "Effective medium theory of thin-plate acoustic metamaterials," *Journal of the Acoustical Society of America*, vol. 135, no. 4, pp. 1844–1852, 2014.

[3] J. Vazquez Torre, J. Brunskog, and V. Cutanda Henriquez, "An analytical model for broadband sound transmission loss of a finite single leaf wall using a metamaterial," *Journal of the Acoustical Society of America*, vol. 147, no. 3, pp. 1697–1708, 2020.

[4] J. Vazquez Torre, J. Brunskog, V. Cutanda Henriquez, and J. Jung, "Hybrid analytical-numerical optimization design methodology of acoustic metamaterials for sound insulation," *Journal of the Acoustical Society of America*, vol. 149, no. 6, pp. 4398–4409, 2021.

[5] L. Van Belle, C. Claeys, E. Deckers, and W. Desmet, "On the impact of damping on the dispersion curves of a locally resonant metamaterial: Modelling and experimental validation," *Journal of Sound and Vibration*, vol. 409, pp. 1–23, 2017.

[6] L. Van Belle, C. Claeys, E. Deckers, and W. Desmet, "The impact of damping on the sound transmission loss of locally resonant metamaterial plates," *Journal of Sound and Vibration*, vol. 461, p. 114909, 2019.

[7] Y. Chen, M. Barnhart, J. Chen, G. Hu, C. Sun, and G. Huang, "Dissipative elastic metamaterials for broadband wave mitigation at subwavelength scale," *Composite Structures*, vol. 136, pp. 358–371, 2016.

[8] D. Roca, J. Cante, O. Lloberas-Valls, T. Pàmies, and J. Oliver, "Multiresonant layered acoustic metamaterial (MLAM) solution for broadband low-frequency noise attenuation through double-peak sound transmission loss response," *Extreme Mechanics Letters*, vol. 47, p. 101368, 2021.

[9] C. Claeys, N. Rocha de Melo Filho, L. Van Belle, E. Deckers, and W. Desmet, "Design and validation of metamaterials for multiple structural stop bands in waveguides," *Extreme Mechanics Letters*, vol. 12, pp. 7–22, 2017.

[10] S. Janssen, L. Van Belle, N. de Melo Filho, W. Desmet, C. Claeys, and E. Deckers, "Improving the noise insulation performance of vibro-acoustic metamaterial panels through multi-resonant design," *Applied Acoustics*, vol. 213, p. 109622, 2023.

[11] D. Giannini, M. Schevenels, and E. Reynders, "Rotational and multimodal local resonators for broadband sound insulation of orthotropic metamaterial plates," *Journal of Sound and Vibration*, vol. 547, no. 117453, pp. 1–17, 2023.

[12] D. Giannini and E. Reynders, "Effective medium modelling of real-world multi-modal metamaterial panels achieving broadband vibroacoustic attenuation," *Extreme Mechanics Letters*, vol. 69, p. 102161, 2024.

[13] A. Santoni, S. Schoenwald, B. Van Damme, and P. Fausti, "Determination of the elastic and stiffness characteristics of cross-laminated timber plates from flexural wave velocity measurements," *Journal of Sound and Vibration*, vol. 400, pp. 387–401, 2017.

[14] D. Giannini and E. P. B. Reynders, "Optimized multimodal rotational resonators for enhanced sound insulation in metamaterial cross-laminated timber panels," in *Proceedings of the 31st International Conference on Noise and Vibration Engineering, ISMA 2024* (W. Desmet, B. Pluymers, D. Moens, and S. Neeckx, eds.), (Leuven, Belgium), p. 261–274, September 2024.

[15] International Organization for Standardization, *ISO 10140-2: Acoustics – Laboratory measurement of sound insulation of building elements – Part 2: Measurement of airborne sound insulation*, 2021.

[16] Y. Yang, B. Mace, and M. Kingan, "Vibroacoustic analysis of periodic structures using a wave and finite element method," *Journal of Sound and Vibration*, vol. 457, pp. 333–353, 2019.

[17] Y. Yang, C. Fenemore, M. Kingan, and B. Mace, "Analysis of the vibroacoustic characteristics of cross laminated timber panels using a wave and finite element method," *Journal of Sound and Vibration*, vol. 494, no. 115842, pp. 1–20, 2021.

[18] C. Claeys, P. Sas, and W. Desmet, "On the acoustic radiation efficiency of local resonance based stop band materials," *Journal of Sound and Vibration*, vol. 333, no. 14, pp. 3203–3213, 2014.

[19] International Organization for Standardization, *ISO 717-1: Acoustics – Rating of sound insulation in buildings and of building elements – Part 1: Airborne sound insulation*, 2013.